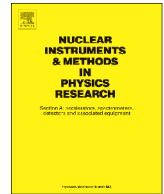




Contents lists available at ScienceDirect

Nuclear Instruments and Methods in Physics Research A

journal homepage: www.elsevier.com/locate/nima

TCAD simulation of Low Gain Avalanche Detectors



Ranjeet Dalal, Geetika Jain, Ashutosh Bhardwaj*, Kirti Ranjan

Center for Detector & Related Software Technology (CDRST), Department of Physics and Astrophysics, University of Delhi, India

ARTICLE INFO

Article history:

Received 9 December 2015

Received in revised form

28 July 2016

Accepted 24 August 2016

Available online 26 August 2016

Keywords:

Detector modeling and simulations

Radiation hard detectors

Low Gain Avalanche Detector

ABSTRACT

In the present work, detailed simulation using Technology Computer Aided Design (TCAD) tool, Silvaco for non-irradiated and irradiated LGAD (Low Gain Avalanche Detector) devices has been carried out. The effects of different design parameters and proton irradiation on LGAD operation are discussed in detail. An already published effective two trap bulk damage model is used to simulate the radiation damage without implementing any acceptor removal term. The TCAD simulation for irradiated LGAD devices produce decreasing gain with increasing fluence, similar to the measurement results. The space charge density and electric field distribution are used to illustrate the possible reasons for the degradation of gain of the irradiated LGAD devices.

© 2016 Elsevier B.V. All rights reserved.

1. Introduction

Recently proposed Low Gain Avalanche Detector (LGAD) designs have been the subject of increasing interest within the silicon (Si) sensor community [1–5]. The possibility of controlled avalanche in these devices would allow the fabrication of thinner Si sensors, thus reducing the material budget and the operating voltage for future applications [1,2]. The LGAD devices fabricated by CNM (Barcelona) have shown promising characteristics before irradiation [2]. But, after hadron irradiation, a significant degradation of gain (charge multiplication) has been observed in these devices. These results have not been explained by earlier simulations and are attributed to the possible acceptor removal with irradiation [1]. The charge multiplication process in these devices can be useful in designing the thinner Si sensors with output signals similar to the standard thicker sensors. Moreover, these devices can be considered as ideal candidates for ultrafast sensors [2]. The signal gain (charge multiplication) in these devices is due to the very high electric field region created by depositing moderate doping density of boron layer or p-well, under the n^+ implant in n-on-p Si sensors (resulting in so-called $n^+ + p^+ - p$ configuration). The basic charge multiplication mechanism in these devices is similar to the principle of the avalanche photodiodes [6,7]. The presence of a high electric field in the multiplication region results in higher gain but it can affect the breakdown voltage adversely. Thus, the gain in LGAD devices is strongly

influenced by the n^+ and p-well doping profiles and hence these doping profiles must be carefully tuned to obtain a required gain with a sufficiently high breakdown voltage (> 1000 V). A few TCAD simulation works have already investigated the effect of the p-well dose on gain and breakdown of non-irradiated LGAD devices [1,6].

In Section 3, we will investigate the gain as a function of the exact p-well profile, not just the peak doping density. In addition, the effect of the n-well doping profile will be considered.

If the LGAD devices qualify to be used in the tracker of high luminosity collider experiments, these detectors will be exposed to extremely harsh radiation scenario and face both neutral (mainly neutrons) and charged (protons and pions) hadron environment. It has been observed that the gain of 300 μm thick devices decreases sharply with fluence [1,3,8] and becomes very low (or almost negligible) for fluence greater than $5 \times 10^{14} \text{ n}_{\text{eq}} \text{ cm}^{-2}$. This performance has not been properly understood. It may be interesting to note that earlier simulation studies have indicated that the electric field inside the p-trench region (or p-well) would remain almost same with fluence and hence gain would not be affected by the irradiation [1,6], contradicting the experimental data. Recently, the acceptor removal mechanism has been suggested as a possible explanation for the lowering of gain with fluence in LGAD devices [1,3,8], however, it is not yet successfully implemented in any TCAD simulation framework. In Section 2.2, we will introduce realistic radiation damage model and investigate the effect of proton radiation on the gain of LGAD devices.

* Corresponding author.

E-mail address: ashutosh.bhardwaj@cern.ch (A. Bhardwaj).

2. Simulation structures and bulk damage model

2.1. Simulation structure

The TCAD simulations are performed on a p-type Si substrate with a uniform bulk doping concentration of $1 \times 10^{12} \text{ cm}^{-3}$. The gain of the LGAD devices are simulated using a plane parallel 2-D structure with a width of $80 \mu\text{m}$ and a thickness of $300 \mu\text{m}$. The Gaussian profile is used for n^+ implantation and p-well implantation (on the top side). If not otherwise specified, the peak doping density for the n^+ (N_n) is kept at $1 \times 10^{18} \text{ cm}^{-3}$ with an implant diffusion depth (d_n) of $4 \mu\text{m}$ (having 1 Gaussian $\sigma = 0.76 \mu\text{m}$), while the peak doping density for p-well (N_p) is kept at $9.75 \times 10^{16} \text{ cm}^{-3}$ with an implant diffusion depth (d_p) of $7 \mu\text{m}$ (which corresponds to a p-well dose of $1.78 \times 10^{13} \text{ cm}^{-2}$ and $\sigma = 1.46 \mu\text{m}$). For a given implant diffusion depth ($d_{n,p}$) and peak doping density ($N_{n,p}$), Gaussian σ can be estimated by the relation given below:

$$\sigma = \frac{d_{n,p}}{\sqrt{-2 \cdot \ln\left(\frac{R}{N_{n,p}}\right)}}$$

where R denotes the reference or bulk doping density of the device. For all the doping profiles used in the present work, a table is provided in the Appendix A listing the values of Gaussian σ for corresponding values of implant diffusion depth and peak doping density of the device. It may be noted from the implant profile shown in Fig. 1(b) that the n^+ /p-well junction depth is a function of both n^+ and p-well doping profiles and is less than the value of d_n . The backside p^+ contact is implemented using the peak doping concentration of $1 \times 10^{18} \text{ cm}^{-3}$ and implant diffusion depth of $2 \mu\text{m}$ ($\sigma = 0.38 \mu\text{m}$) with the gaussian profile. A zoomed view of the n^+ and p-well region of the simulation structure is shown in Fig. 1(a). Fig. 1(b) shows the doping profile along the depth of the detector (near the multiplication region). The gain simulation for these devices is carried out using a $1 \mu\text{m}$ wide front side infrared laser pulse of wavelength 1060 nm . The laser power density of 1 W cm^{-2} and 100 ps duration is used. A device area factor of 2×10^5 is used in the simulation which acts as a multiplicative factor in the signal output for transient simulations. Metal contacts are removed from the entry and exit points of the laser to avoid reflection. Signal simulation is carried out using mix-mode simulation in which external circuit elements of a bias-tee are

implemented. The bias-tee resistance of $3.1 \text{ k}\Omega$ and capacitance of 2.2 nF are used to extract the transient signal through 50Ω resistance. The LGAD gain is defined as the ratio of the collected charge (calculated by integrating TCT signal pulse) for a LGAD device and that of the reference diode (without the p-well). All the design parameters of the reference diode, including the doping of n^+ and its implant diffusion depth, are kept similar to the LGAD devices for comparison purposes. The breakdown voltage is simulated by keeping the width of the p-well ($58 \mu\text{m}$) less than the width of the n^+ implant ($80 \mu\text{m}$) and by including an additional junction termination extension (JTE) structure.

Silvaco TCAD solves the continuity and Poisson's equation for the charge carriers. The default parameters were used for the concentration-dependent lifetime, Shockley-Read-Hall (SRH) recombination and for concentration and field dependent mobility models. The Selberherr impact ionization model is included in the simulation. The simulations are performed using a triangular grid generated by the DevEdit (Silvaco). Reflecting Neumann conditions are imposed at the outer edges of the structure and also on the top of SiO_2 .

2.2. Radiation damage model

In order to explain the measurements and predict the behavior of $300 \mu\text{m}$ thick LGAD devices in the challenging radiation scenario, it is important to include an appropriate radiation damage model within the simulation software. In our previous work, it has been shown that the various effects of proton irradiation can be explained in terms of acceptor and donor trap generation due to irradiation [9,10]. The effective trap model [10] reproduces the correct leakage current, the full depletion voltage and the charge collection efficiency of the Si sensors (reference devices without additional p-well layer) irradiated with the proton fluence up to $2 \times 10^{15} \text{ n}_{\text{eq}} \text{ cm}^{-2}$. This simulation model incorporates one acceptor and one donor trap. For both the traps, a uniform trap distribution is assumed inside the sensor bulk. The trap parameters, like the trap energy levels with respect to the conduction or valance bands (for the acceptor and donor traps respectively), introduction rates (g_{int}) for proton fluence and electron/hole capture cross sections (σ_e/σ_h) are listed in Table 1. All the fluence and introduction rates are normalized to 1 MeV neutron equivalent fluence following the NIEL (Non Ionizing Energy Loss) hypothesis. The surface damage is implemented using appropriate oxide charge density and interface trap densities as described in Ref. [10]

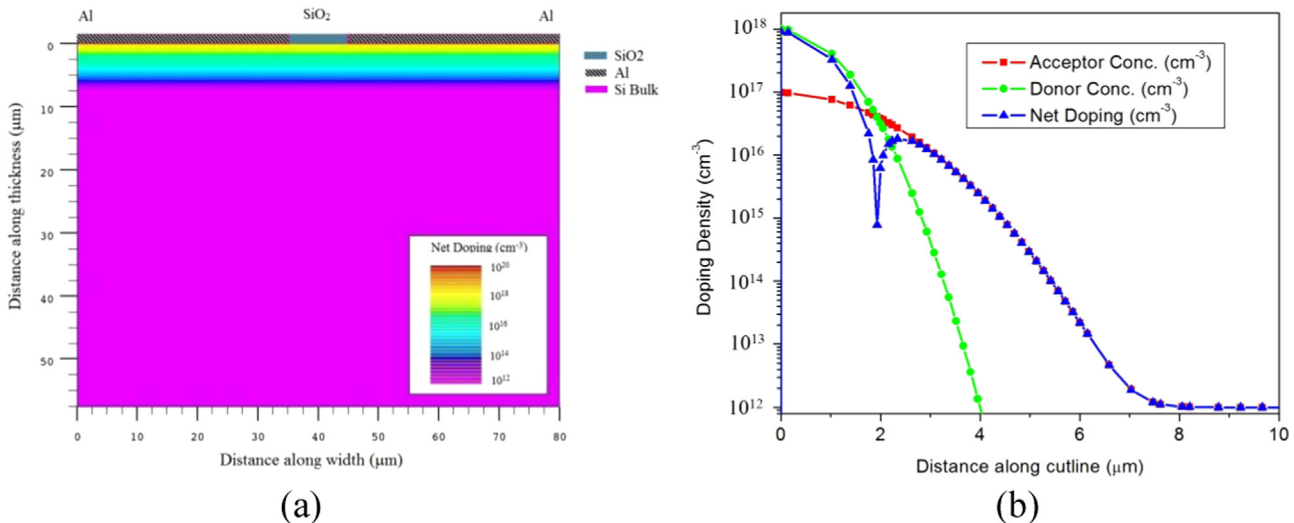


Fig. 1. (a) 2-D zoomed-in net doping profile around the n^+ /p-well region of the simulated LGAD structure having width $80 \mu\text{m}$. A $10 \mu\text{m}$ wide SiO_2 window is used for infrared laser TCT simulation. (b) 1-D doping profile of the n^+ implant, p-well and net doping along the vertical cut line through the depth of the device.

Table 1
Two trap level model parameters [10].

No.	Trap	Energy Level	g_{int} (cm ⁻¹)	σ_e (cm ²)	σ_h (cm ²)
1.	Acceptor	$E_c - 0.51$ eV	4	2×10^{-14}	3.8×10^{-15}
2.	Donor	$E_v + 0.48$ eV	3	2×10^{-15}	2×10^{-15}

for simulating the breakdown voltage for the irradiated devices. However, for simulating the gain of the LGAD devices the surface damage is not important since the gain is due to the localized high electric field in the bulk near the p+ well region.

3. Performance of non-irradiated LGAD devices

Fig. 2(a) shows the signal generated in the LGAD device for an applied bias (V_{bias}) of 200 V when the laser (infrared) is shone on the top surface. The total charge is calculated by integrating the signal over a time period of 25 ns. The device gain is defined as the ratio of the charge collected by the LGAD device to that collected by the reference diode (same device without p-well). Fig. 2 (b) shows the representative plot of the gain as a function of V_{bias} considering different p-well doses by varying the N_p while keeping other parameters constant. On the basis of the achieved gain, these LGAD devices are labeled as low gain (~2.5 at 200 V for a dose of 1.61×10^{13} cm⁻²), moderate gain (~5 at 200 V for a dose of 1.78×10^{13} cm⁻²) and high gain (~15 at 200 V for a dose of 1.87×10^{13} cm⁻²). For the low and moderate gain devices, there are two visibly distinct regions: steep increment with V_{bias} before full depletion, and a gradually increasing plateau region for higher biases. However, for the high gain structure, the plateau region no longer remains constant and its slope increases sharply with increase in gain. The simulated moderate gain variation with V_{bias} is similar to the ones reported in earlier work [1,3,8], whereas that of the low gain is similar to the measurements shown in Ref. [8,12]. Fig. 3 shows the typical IV characteristics of the representative LGAD device. For comparison purposes, a plot of the reference diode is also shown. The breakdown voltage (V_{BD}) is defined by a sharp increase in the leakage current.

As mentioned above, the characteristics of the LGAD devices are strongly dependent on the doping profiles of n⁺ implant and p-well. A careful tuning of both the profiles is imperative to

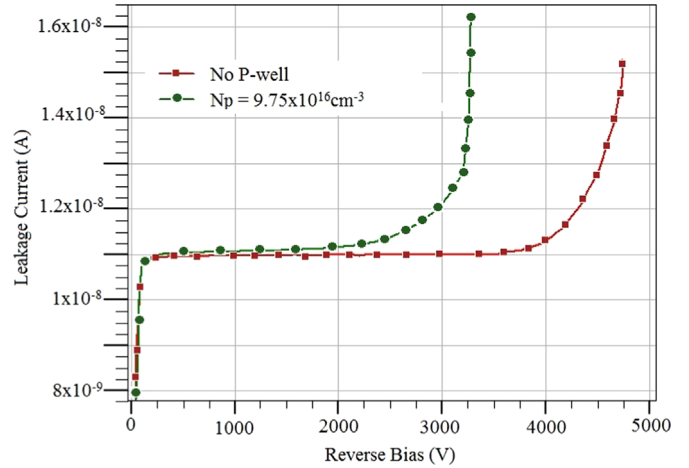


Fig. 3. The IV characteristics of reference diode and LGAD structure (moderate gain) at T=263 K.

achieve the desired performance. A systematic study of the variation of these profiles on the gain and V_{BD} is provided in following sub-sections. It may be noted that the actual V_{BD} and its location are sensitive to the layout of the JTE structure. The V_{BD} study of the LGAD diodes, which strongly depends on the JTE structure, is beyond the scope of this article. Hence, the results concerning the V_{BD} in this work should be considered more as a qualitative indication than a truly quantitative estimate.

3.1. Effect of p-well doping profile

As mentioned earlier, the p-well dose can be varied by changing either N_p (keeping d_p fixed) or d_p (while keeping N_p fixed) or both. We have studied several possible cases for both the variations. Fig. 4(a) shows a plot of the gain and the V_{BD} vs. N_p (or dose) while keeping the d_p fixed. It can be seen that the gain remains almost unity up to N_p of 7.6×10^{16} cm⁻³ and increases sharply with increase in N_p , reaching to a value of 15 for N_p value equal to 1.025×10^{17} cm⁻³. The increase in the gain with the p-well dose is attributed to an increase in the electric field around the n⁺/p-well junction, as shown in Fig. 4(b). The overall sensor gain depends on the magnitude of the electric field as well as the width of the high field region [7] around the n⁺/p-well junction. Since the width of

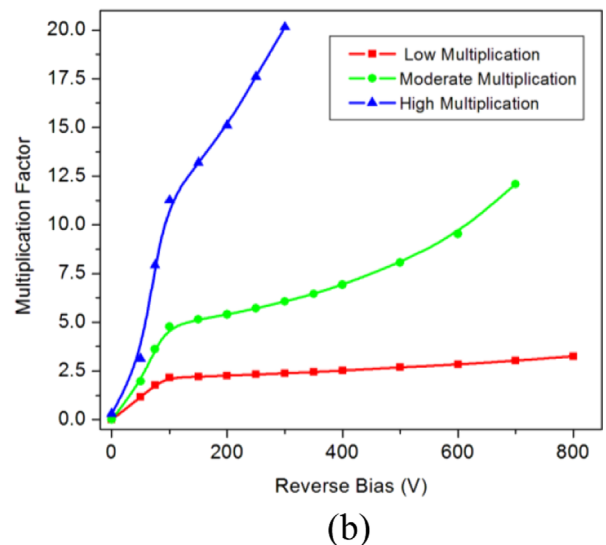
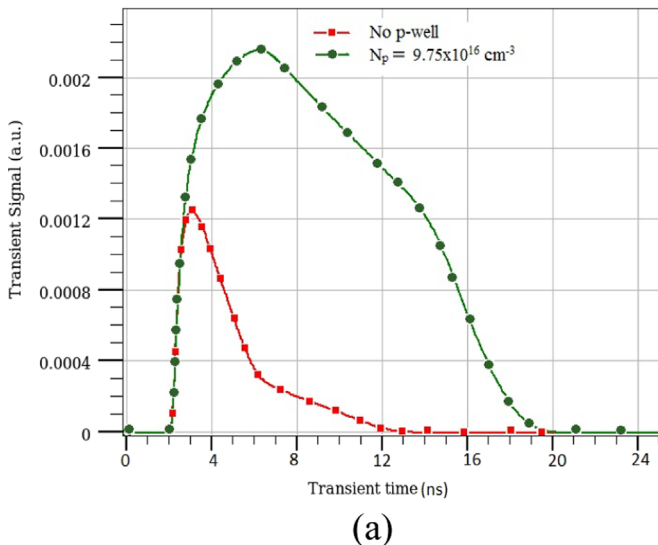


Fig. 2. (a) The transient signal output for reference diode and LGAD structure with $N_p = 9.75 \times 10^{16}$ cm⁻³ (or dose of 1.78×10^{13} cm⁻²) at $V_{bias} = 200$ V. (b) Gain vs. V_{bias} for three different values of doses using $d_p = 7$ μ m.

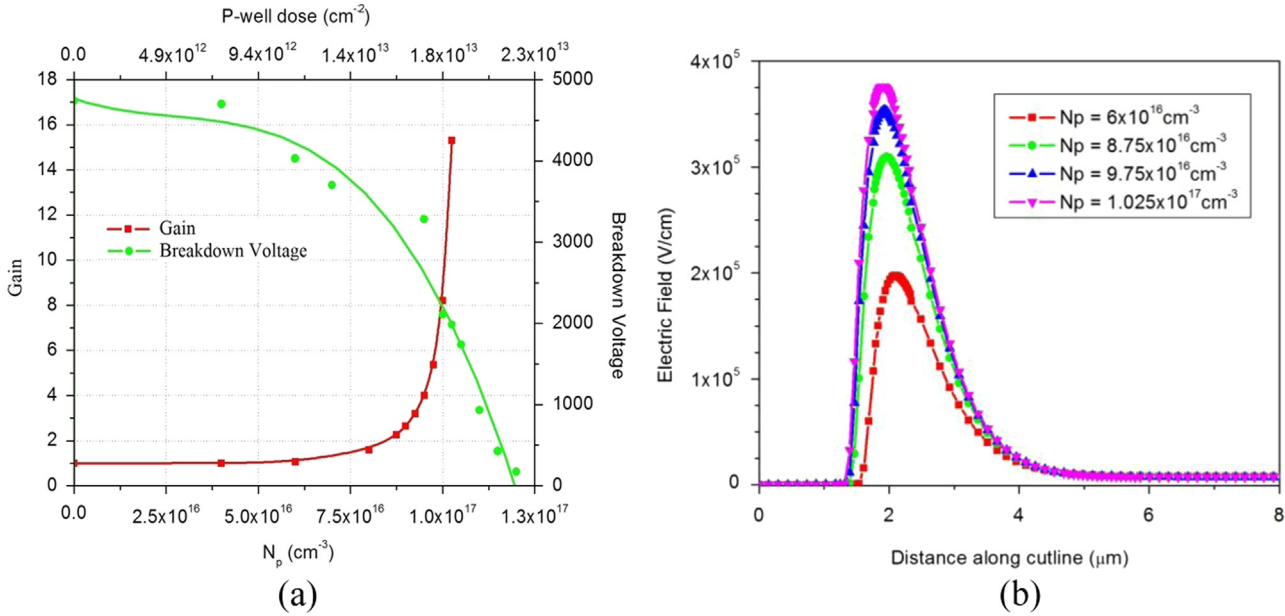


Fig. 4. (a) Gain at $V_{bias}=200$ V and V_{BD} variation vs. N_p . (b) Simulated electric field near the p-well region for different N_p at $V_{bias}=200$ V. Following parameters are used for these simulations: $d_p=7$ μm, $N_n=1 \times 10^{18}$ cm⁻³, $d_n=4$ μm and $T=263$ K.

the high field region is only few micron for LGAD devices, the peak electric field should be around 3×10^5 V/cm or more for a significant gain. It can be seen from Fig. 4(b) that the peak electric field in the multiplication region is about 3×10^5 V/cm for the low multiplication case and reaches about 3.6×10^5 V/cm for the high gain scenario. The higher gain achieved in LGAD devices, however, is at the expense of the reduced V_{BD} , as shown in Fig. 4(a). It may be noted that the V_{BD} of 2000 V is achieved for the N_p of $\sim 1.025 \times 10^{17}$ cm⁻³ (corresponding to the gain of 15).

Further, similar variation was studied for different values of d_p . Fig. 5(a) shows the plot of gain vs. d_p for different values of N_p . It can be seen that the gain of LGAD device is also affected by varying d_p , while keeping the N_p constant. For these N_p values, the gain remains constant for a minimum d_p , beyond which it increases sharply. Increase in the d_p (for a given N_p) results in higher

acceptor density and hence leads to the higher electric field around the n^+/p -well junction (Fig. 5(b)), leading to the increase in gain. For a given d_p , the gain increases with increase in N_p beyond a minimum d_p .

To illustrate the relevance of doping profile (as opposed to total p-well dose only) in tailoring the gain of the LGAD devices, Table 2 lists the gain (in parentheses) and p-well dose values for different combinations of N_p and d_p . It may be noted from this Table that a dose of about 1.6×10^{13} cm⁻² can be attained using (a) $N_p=8.75 \times 10^{16}$ cm⁻³ with $d_p=7.1$ μm or (b) $N_p=1.025 \times 10^{17}$ cm⁻³ with $d_p=6$ μm. However, these two combinations (for the same p-well dose) give significantly different gains, i.e. 3.2 and 1 respectively. Similar observations can be made for another dose of 1.81×10^{13} cm⁻², which, for the combination of $N_p=9.75 \times 10^{16}$ cm⁻³ and $d_p=7.1$ μm gives a gain of 19.5 whereas

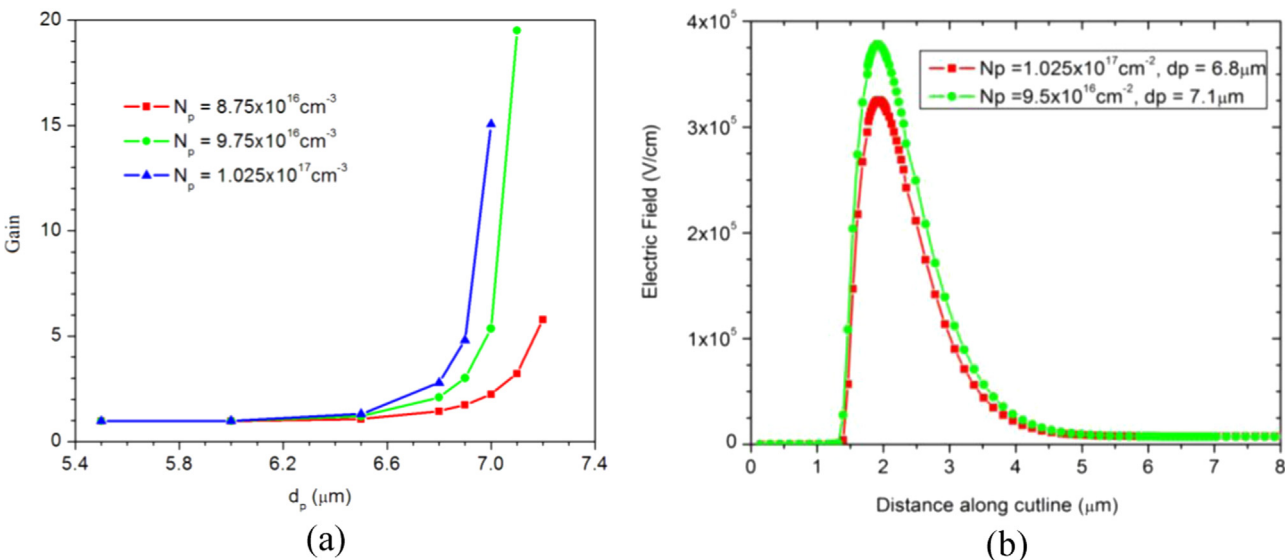


Fig. 5. (a) Variation of the gain vs. d_p for the different values of N_p , and (b) electric field variation around n^+/p -well junction for two different p-well profiles. Following parameters are used for these simulations: $N_n=1 \times 10^{18}$ cm⁻³, $d_n=4$ μm, $V_{bias}=200$ V and $T=263$ K.

Table 2

Dose values and gain (in parentheses) for different values of N_p and d_p . Following parameters are used for these simulations: $N_n=1 \times 10^{18} \text{ cm}^{-3}$, $d_n=4 \text{ }\mu\text{m}$, $V_{\text{bias}}=200 \text{ V}$ and $T=263 \text{ K}$.

$N_p \text{ (cm}^{-3}\text{)}$	p-well dose in cm^{-2} (gain)				
	$d_p=5.5 \text{ }\mu\text{m}$	$d_p=6 \text{ }\mu\text{m}$	$d_p=6.5 \text{ }\mu\text{m}$	$d_p=6.8 \text{ }\mu\text{m}$	$d_p=7.1 \text{ }\mu\text{m}$
8.75×10^{16}	1.26×10^{13} (1.0)	1.38×10^{13} (1.0)	1.49×10^{13} (1.1)	1.56×10^{13} (1.4)	1.63×10^{13} (3.2)
9.75×10^{16}	1.40×10^{13} (1.0)	1.53×10^{13} (1.0)	1.66×10^{13} (1.2)	1.73×10^{13} (2.1)	1.81×10^{13} (19.5)
1.025×10^{17}	1.47×10^{13} (1.0)	1.60×10^{13} (1.0)	1.74×10^{13} (1.3)	1.82×10^{13} (2.8)	1.90×10^{13} (-)

for the other combination, i.e. $N_p=1.025 \times 10^{17} \text{ cm}^{-3}$ and $d_p=6.8 \text{ }\mu\text{m}$ gives a gain of only 2.8.

It may be concluded that for the set of (N_p, d_p) values considered in this work, low values of p-well doses are insufficient to provide the gain, however, beyond a minimum dose, a combination of high d_p and low N_p provides higher gain. One may need to investigate this further by expanding the parameter space.

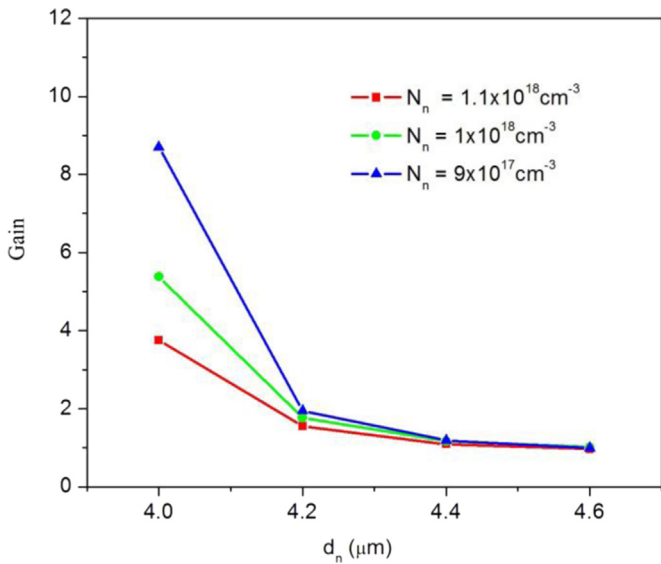


Fig. 6. Gain vs. d_n for LGAD structures for three different values of N_n . Following parameters are used for these simulations: $N_p=9.75 \times 10^{16} \text{ cm}^{-3}$, $d_p=7 \text{ }\mu\text{m}$, $V_{\text{bias}}=200 \text{ V}$ and $T=263 \text{ K}$.

3.2. Effect of n^+ doping profile

The variation of n^+ doping profile (N_n and d_n) also affects the n^+ /p-well junction and region around it, and hence it affects the gain and electric field distribution for a given p-well dose. An increase in d_n (for a given N_n) would shift the n^+ /p-well junction slightly deeper where the p-well doping density would be lower. This leads to decrease in the electric field (and hence the gain) as shown in Fig. 6. Similarly, an increase in the N_n (for a given d_n) would shift the n^+ /p-well junction location deeper inside the Si bulk where the p-well doping density is lower. This results in lower gain as shown in Fig. 6.

Figs. 7(a) and (b) show the net doping profile and electric field distribution respectively, for a fixed n^+ dose for two different combinations of N_n and d_n , i.e. (a) $N_n=9 \times 10^{17} \text{ cm}^{-3}$ and $d_n=4.4 \text{ }\mu\text{m}$ and (b) $N_n=1 \times 10^{18} \text{ cm}^{-3}$ and $d_n=4.0 \text{ }\mu\text{m}$. The former gives a gain of 1.0 while the latter gives a gain of 5.5. Thus, it may be concluded that, for the given set of (N_n, d_n) values considered in this work, a judicious combination of the N_n and the d_n , as opposed to the total n^+ dose, would give an expected gain for the LGAD device.

4. Effect of irradiation on LGAD devices

A systematic analysis of the proton irradiation effect on the LGAD devices is carried out using our bulk damage model [10] within Silvaco framework [11]. As categorized earlier in Fig. 3, the effect of proton fluence is studied for the low gain, medium gain, and high gain LGAD devices. The variation of the gain with V_{bias} for different fluence values is shown in Fig. 8(a), (b) and (c) for

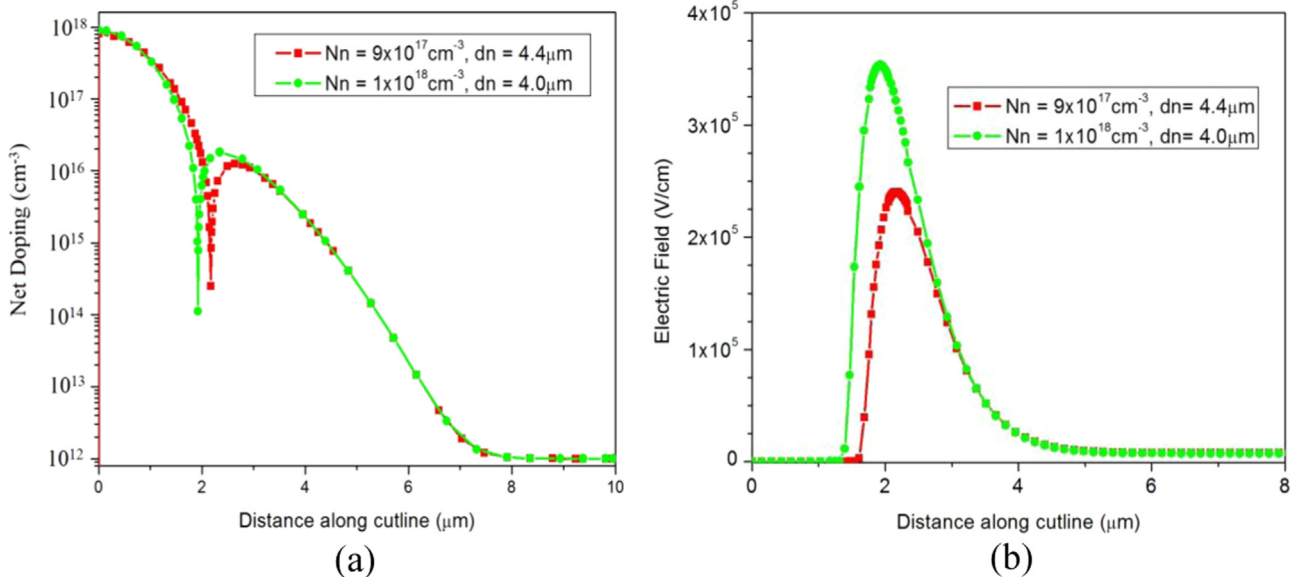


Fig. 7. (a) Doping profile and (b) Electric field along the depth near the p-well region. Following parameters are used for these simulations: $N_p=9.75 \times 10^{16} \text{ cm}^{-3}$, $d_p=7 \text{ }\mu\text{m}$, $V_{\text{bias}}=200 \text{ V}$ and $T=263 \text{ K}$.

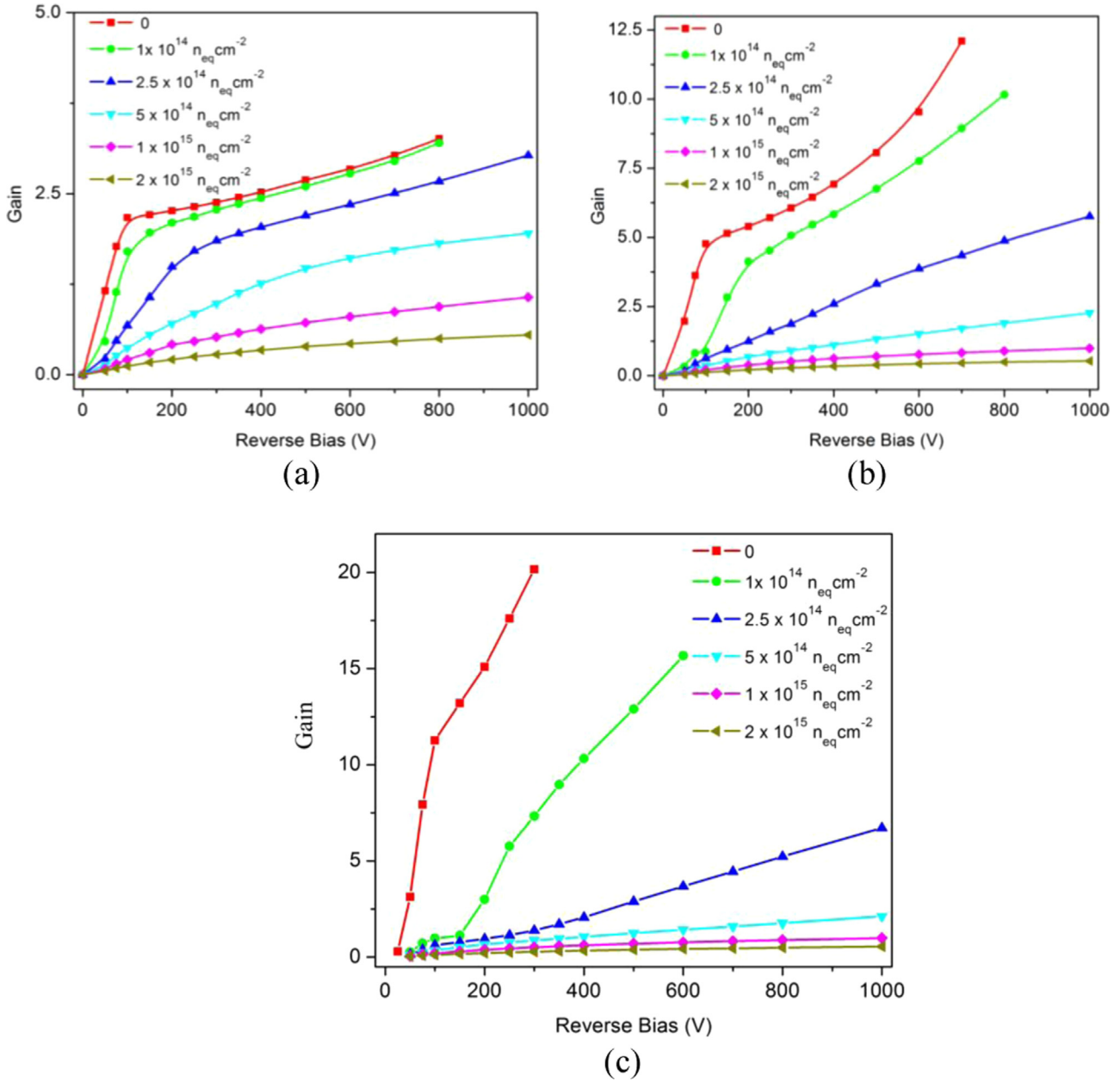


Fig. 8. The gain vs. V_{bias} for different fluence values for (a) low gain (dose of $1.61 \times 10^{13} \text{ cm}^{-2}$), (b) moderate gain (dose of $1.78 \times 10^{13} \text{ cm}^{-2}$), and (c) high gain (dose of $1.87 \times 10^{13} \text{ cm}^{-2}$) at $T=253 \text{ K}$.

different categories. The general trend of the plots for the irradiated devices is similar to that observed for the non-irradiated ones, but, it may be seen that the gain is reduced with an increase in fluence and it even decreases below that of the non-irradiated reference diode for higher fluence values. Moreover, the onset of plateau region also occurs at slightly higher applied bias.

A comparison of the gain vs. fluence for all three cases at $V_{\text{bias}}=300 \text{ V}$ and 800 V are shown in Fig. 9(a) and (b) respectively. Although the initial value of the gain in the moderate and high gain for non-irradiated LGAD devices are higher but, it decreases sharply with irradiation and becomes comparable to the low gain LGAD devices for a fluence of about $5 \times 10^{14} \text{ n}_{\text{eq}} \text{ cm}^{-2}$. This behavior is consistent with the recent measurements of the LGAD devices, irradiated with charged hadrons [8].

The simulated leakage current variation with the fluence is shown in Fig. 10(a) and (b) for the low gain and the moderate gain LGAD structures respectively. These plots are qualitatively similar to the measurements reported in Ref. [8]. It can be observed that,

contrary to the reference diodes, leakage currents in LGAD structures are not linearly proportional to the fluence. Moreover, the leakage current of LGAD devices is about 1.5–5 times higher (depending on fluence) than that of the reference diodes. This implies that along with the usual charge carrier generation/recombination process due to the bulk traps (which creates leakage current linearly proportional to fluence), additional current is generated in the multiplication layer.

The effect of the proton irradiation on the gain for the different gain scenario can be understood in terms of irradiation effect on electric field profile inside the irradiated LGAD sensors. For the different values of fluence, the electric field variation inside the p-well region is shown in Fig. 11(a) while its variation into the sensor bulk is shown in Fig. 11(b). The electric field profile is plotted for the moderate gain scenario at $V_{\text{bias}}=500 \text{ V}$ and $T=253 \text{ K}$. It can be observed from Fig. 11(a) that the peak value and the width of the electric field distribution inside the p-well region decrease with increase in fluence, which would affect the

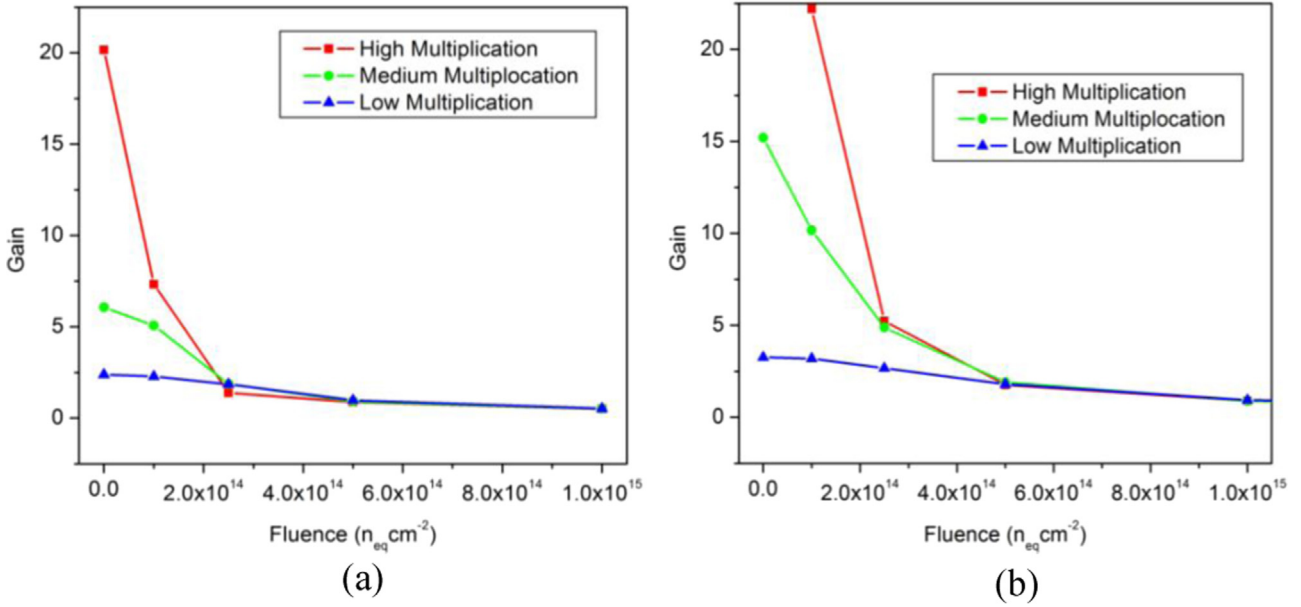


Fig. 9. The gain variation vs. fluence for the different gain scenario at the reverse bias voltage (a) of 300 V, and (b) of 800 V at 253 K.

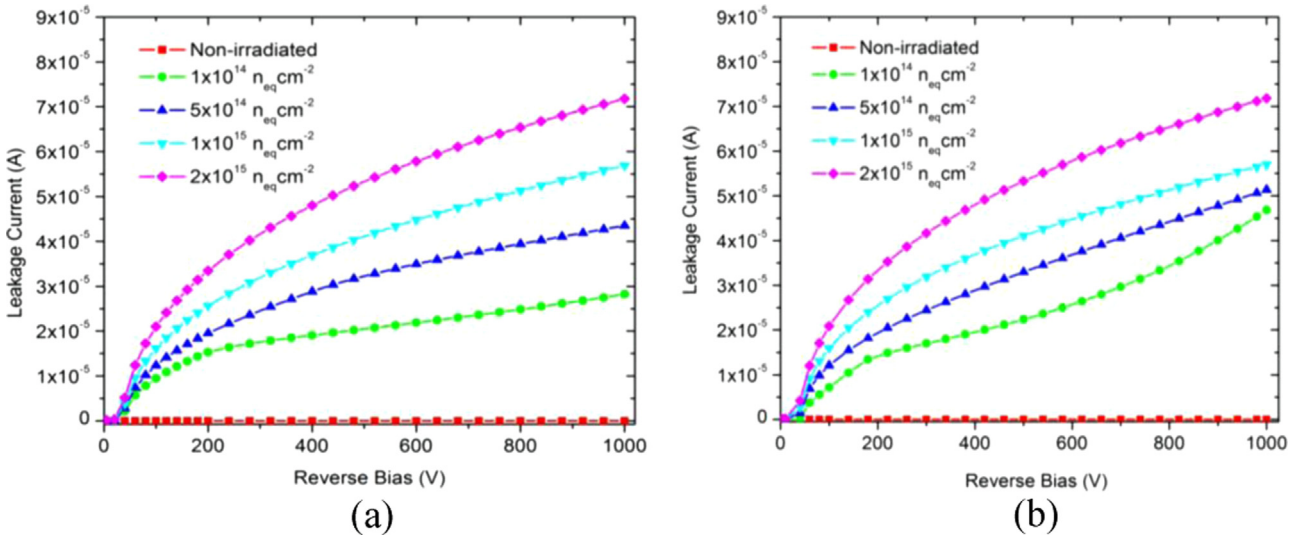


Fig. 10. The leakage current (for the active area of $1 \text{ cm} \times 1 \text{ cm}$) variation vs. fluence (a) for the low gain and (b) for the moderate gain scenario at 253 K.

gain of the LGAD device. Moreover, the electric field near the p⁺ backside grows with the increase in fluence due to the double junction effect [13–15], leaving lower values of the electric field inside the sensor bulk. Particularly, there is very low electric field region just below the p-well region, which leads to an inefficient transfer of electrons (for higher fluence values) to the multiplication region. Hence, lowering of the electric field around the n⁺/p-well junction as well as in the bulk (below p-well) leads to very low or no gain for irradiated LGAD designs.

The effective space charge density inside the LGAD devices is strongly affected by the hadron irradiation. As shown in Fig. 10, the additional current component comes from the charge multiplication around the n⁺/p-well junction after irradiation. Since the n⁺/p-well junction is near the n⁺ electrode, the additional holes travel almost whole of the device bulk before getting collected at the p⁺ electrode and thus would lead to predominately donor trap filling in the sensor bulk. The effective space charge density (n-type doping density + ionized donor trap density – p-type doping density – ionized acceptor trap density) for the moderate gain LGAD device is shown in Fig. 12(a) and (b). It can be seen that the sensor bulk

becomes effectively donor type after irradiation [16] and the effective space charge density of the p-well is also affected. It may be noted that we have not used acceptor removal parameterization [8] in our simulation and the variation of the electric field, the leakage current, the effective space charge density and the gain with irradiation is only a manifestation of acceptor/donor traps effect.

The present simulation work is meant for the proton irradiated LGAD devices but neutron irradiation would also induce the similar gain lowering. Most of the traps due to the neutron and proton irradiation are quite similar [17] but the neutron irradiation induces fewer donor traps (particularly E30 trap) which would result in lower backside electric field [10] peak, near p⁺. This would result in the slightly higher field towards the p-well side or slightly efficient electron collection for neutron irradiated sensors, resulting in a higher gain. This has been observed experimentally as well [8].

5. Summary

We have presented simulation results for the LGAD devices. The simulation predictions provide a reasonable qualitative description

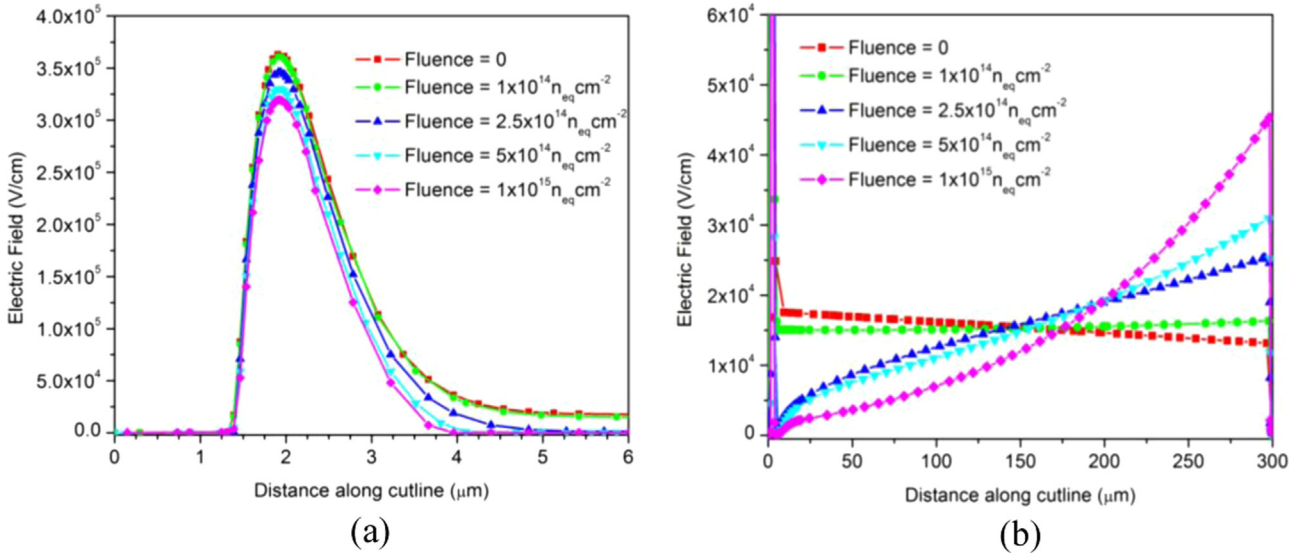


Fig. 11. The electric field for different irradiation fluence (a) for $V_{\text{bias}}=500$ V around the multiplication region, and (b) inside the sensor volume for $N_p=9.75 \times 10^{16} \text{ cm}^{-3}$ (moderate gain case) at $T=253$ K.

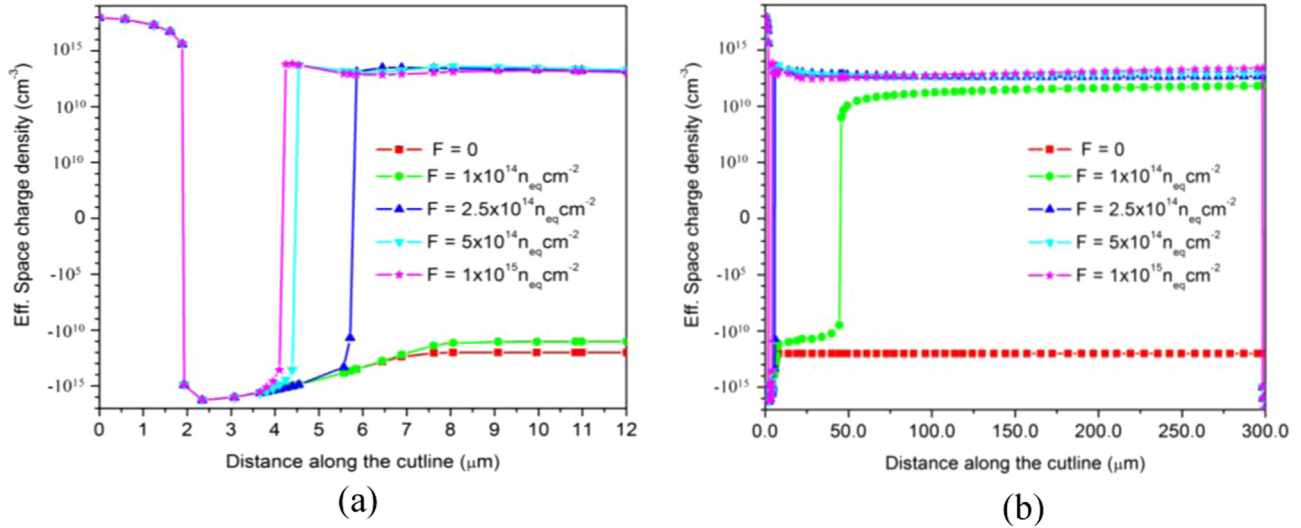


Fig. 12. The effective space charge density for different irradiation fluence (a) around the multiplication region, and (b) inside the sensor volume for $N_p=9.75 \times 10^{16} \text{ cm}^{-3}$ (moderate gain case) at $T=253$ K for $V_{\text{bias}}=500$ V.

of both the non-irradiated and irradiated LGAD device behavior. It has been emphasized that the gain of the non-irradiated LGAD devices is strongly influenced by the overall doping profiles of the p-well and n^+ implantations. We have studied the (N_p , d_p) parameter space of ($8.75\text{--}10.25 \times 10^{16} \text{ cm}^{-3}$, $5.5\text{--}7.1 \mu\text{m}$) and (N_n , d_n) parameter space of ($0.9\text{--}1.1 \times 10^{18} \text{ cm}^{-3}$, $4.0\text{--}4.6 \mu\text{m}$). It has been found that within the parameter space studied, a minimum p-well dose is required to achieve the desired gain, however, beyond that dose, a combination of high implant diffusion depth and low peak doping concentration of the p-well provides higher gain.

An effective two trap bulk damage model is used to simulate the radiation damage. The incorporated radiation damage model successfully explains the decrease in gain of the LGAD devices with an increase in proton fluence, as observed in measurements. It may be interesting to observe that the gain simulation for irradiated LGAD structures is carried out without changing the acceptor concentration inside the p-well region. The gain variation with fluence seems to be due to the traps effect only, which is further corroborated using the electric field, leakage current and effective space charge density of the irradiated LGAD devices. It

has been found that the space-charge density of the sensor bulk and the p-well regions change in a way such that the sensor bulk becomes effectively donor type after irradiation. Hence, these simulations provide another plausible explanation for the lowering of the gain as opposed to incorporation of only acceptor removal mechanism [8]. Authors would like to emphasize that this work provides a useful insight into the working of LGAD devices, however, further simulation and experimental results are needed to understand and utilize the potential of LGAD devices in the future high energy physics experiments.

Acknowledgments

Authors would like to thank University of Delhi and Department of Science & Technology (DST, India) for providing financial assistance. The work was partly performed in the framework of the RD50 collaboration. RD and GJ would also like to thank UGC for providing financial assistance.

Appendix A

See Table A1.

Table A1

The RMS of the Gaussian implant diffusion profile (σ) for the corresponding values of implant diffusion depth and peak doping density of the device.

$d_{n,p}$ (μm)	$N_{n,p}$ (cm^{-3})	σ (μm)
4	1×10^{18}	0.7610
7	9.75×10^{16}	1.4604
2	1×10^{18}	0.3805
7	7.6×10^{16}	1.4765
7	1.025×10^{17}	1.4572
6.8	1.025×10^{17}	1.4156
7.1	9.5×10^{16}	1.4829
5.5	8.75×10^{16}	1.1529
5.5	9.75×10^{16}	1.1474
5.5	1.025×10^{17}	1.1450
6	8.75×10^{16}	1.2577
6	9.75×10^{16}	1.2518
6	1.025×10^{17}	1.2490
6.5	8.75×10^{16}	1.3625
6.5	9.75×10^{16}	1.3561
6.5	1.025×10^{17}	1.3531
6.8	8.75×10^{16}	1.4254
6.8	9.75×10^{16}	1.4187
7.1	8.75×10^{16}	1.4883
7.1	9.75×10^{16}	1.4812
7.1	1.025×10^{17}	1.4780

References

- [1] G. Pellegrini, et al., Nucl. Instrum. Methods Phys. Res. A 765 (2014) 12–16.
- [2] H.F.W. Sadrozinski, et al., Nucl. Instrum. Methods Phys. Res. A 765 (2014) 7–11.
- [3] G. Kramberger, et al., 24th RD50 Workshop, Bucharest, Romania, 11–13 June 2014.
- [4] G. Dalla Betta, et al., Nucl. Instrum. Methods Phys. Res. A 796 (2015) 154–157.
- [5] I. Vila, et al., ALCW-2015 workshop, KEK Tsukuba, Japan, 20–24 April 2015.
- [6] P. Fernández-Martínez, et al., Nucl. Instrum. Methods Phys. Res. A 658 (2011) 98–102.
- [7] S.M. Sze, K.K. Ng, Physics of Semiconductor Devices, 3rd ed., John Wiley & Sons, Inc, Hoboken, NJ, USA, 2007.
- [8] G. Kramberger et. al., 2015 JINST 10 P0006.
- [9] R. Dalal et al., Simulations of hadron irradiation effects for Si sensors using effective bulk damage model, in: Proceedings of the 24th RD50 Workshop, Bucharest, Romania, 11–13 June 2014.
- [10] R. Dalal et al., Simulation of irradiated Si detectors, in: Proceedings of the 23rd International Workshop on Vertex Detectors, PoS (Vertex2014)030, 2014.
- [11] ATLAS Silvaco version 5.15.32.R Nov, 2009, Users manual (<http://www.silvaco.com>).
- [12] C. Gallrapp et. al., TCT measurements on neutron and proton irradiated LGAD pad sensors, in: Proceedings of the 26th RD50 Workshop, June 2015.
- [13] Z. Li, et al., J. Electron. Mater. 21 (7) (1992) 701.
- [14] V. Eremin, et al., Nucl. Instrum. Methods Phys. Res. A 360 (1995) 458.
- [15] U. Biggeri, et al., Nucl. Instrum. Methods Phys. Res. A 338 (1997) 330.
- [16] G. Kramberger et al., Initial acceptor removal in p-type silicon detectors, Presented at 23rd RD50 Workshop, CERN, Nov. 2013.
- [17] I. Pintilie, et al., Nucl. Instrum. Methods Phys. Res. A 611 (2009) 52–68.